



Cite this: *Mater. Adv.*, 2020, 1, 2003

Received 12th May 2020,  
Accepted 10th August 2020

DOI: 10.1039/d0ma00303d

rsc.li/materials-advances

## Hydrothermally grown novel pyramids of the $\text{CaTiO}_3$ perovskite as an efficient electrode modifier for sensing applications†

Khursheed Ahmad,<sup>a</sup> Praveen Kumar<sup>a</sup> and Shaikh M. Mobin  <sup>abc</sup>

Herein, we report novel  $\text{CaTiO}_3$  pyramids, prepared by a hydrothermal approach using calcium nitrate and titanium butoxide in the presence of sodium hydroxide. The physio-chemical properties of the synthesized  $\text{CaTiO}_3$  pyramids were probed by PXRD, FTIR, BET, SEM and EDX. The synthesized  $\text{CaTiO}_3$  pyramids possess a good specific surface area which is beneficial for electrochemical applications. Thus, the  $\text{CaTiO}_3$  pyramids were applied as an electrode modifier to develop an electrochemical sensor. The working surface area of the glassy carbon (GC) electrode was fabricated with  $\text{CaTiO}_3$  pyramids using the drop casting method. This fabricated electrode was employed to determine urea using the cyclic voltammetry and  $I-V$  techniques. The fabricated electrode exhibited a good detection limit of 1.6  $\mu\text{M}$ .

## 1. Introduction

Urea is present in humans and widely distributed in nature. Urea may cause hepatic failure, urinary tract obstruction, nephritic syndrome, cachexia, dehydration, shock and gastrointestinal problems, if its presence (physiological range 1.33–3.33 mM) changes in the blood serum.<sup>1,2</sup> Urea has good solubility in water and is used as a fertilizer. Due to the good solubility of urea in water it may pollute ground and surface water, which can influence human health.<sup>1</sup> Thus, the detection of urea is necessary. In previous years, conventional methods such as chemiluminescence, electrochemical methods, high performance liquid chromatography, fluorimetry etc. have been widely used for the detection of urea.<sup>3,4</sup> However, the electrochemical technique is found to be one of the most promising approaches for the detection of urea due to its low cost, simplicity, high sensitivity and selectivity.<sup>5–7</sup> The performance of electrochemical sensors depends on the nature of the electrode modifiers.<sup>8–10</sup> Parsaee *et al.*<sup>11</sup> employed a  $\text{NiO-NP}/\text{GO}$  modified GCE for urea sensing and a detection limit of 8  $\mu\text{M}$  was obtained. Mikani *et al.*<sup>12</sup> used an F-doped  $\text{SnO}_2$  electrode modified with  $\text{ZnO-Fe}_3\text{O}_4$ , whereas Sha *et al.*<sup>13</sup> employed graphene–polyaniline for the determination of urea. Naik *et al.*<sup>14</sup> also introduced a nickel sulfide/graphene oxide modified glassy carbon electrode for urea sensing and achieved a

detection limit of 3.79  $\mu\text{M}$ . Bao *et al.*<sup>15</sup> developed a urea sensor using ultrathin nickel–metal–organic framework nanobelts and the detection limit was found to be 2.23  $\mu\text{M}$ . Hahn and co-workers have grown  $\text{ZnO}$  nanorods on Ag/glass and used this for the determination of urea.<sup>16</sup> The above observations indicate that electrode modifiers largely influence the performance of the modified electrodes. Therefore, it would be of great importance to design new electrode modifiers.

Recently, perovskite materials with general molecular formula  $\text{ABO}_3$  have gained enormous attention because of their excellent optoelectronic applications.<sup>17</sup> Perovskite materials have been used in a variety of applications such as solar cells, batteries, photo-detectors, light emitting diodes, sensors, fuel cells and photocatalysis.<sup>18,19</sup> In 2009, He *et al.*<sup>20</sup> prepared  $\text{BaTiO}_3$  perovskite nanocubes for the sensing of hydrogen peroxide. Ahmad *et al.*<sup>21</sup> have synthesized a  $\text{rGO/SrTiO}_3$  composite for the determination of nitro-aromatic compounds. In 2020, Shaikh and co-workers employed an  $\text{N-rGO/SrZrO}_3$  cuboidal composite for electrochemical determination of hydroquinone.<sup>22</sup> Muthukutty *et al.* also introduced  $\text{SrSnO}_3$  as an electrode material for sensing applications.<sup>23</sup>  $\text{CaTiO}_3$  has a perovskite structure and possesses good optoelectronic properties and is widely used in photocatalysis.<sup>24</sup> The surface morphology of  $\text{CaTiO}_3$  may influence its physiochemical properties. Previously,  $\text{CaTiO}_3$  particles were synthesized either by hydrothermal or solvothermal methods. Dong *et al.*<sup>25</sup> have prepared butterfly like dendrites of  $\text{CaTiO}_3$ , whereas Yang *et al.*<sup>26</sup> have obtained  $\text{CaTiO}_3$  hollow micro-cubes. Kimijima *et al.*<sup>24</sup> also synthesized  $\text{CaTiO}_3$  cubic particles with controlled size and shape. Wang *et al.*<sup>27</sup> obtained a  $\text{CaTiO}_3$  nanolamellate using a hydrothermal approach. It is believed that the design and synthesis of nano-materials with new nanostructures are of

<sup>a</sup> Discipline of Chemistry, Indian Institute of Technology Indore, Simrol, Khandwa Road, Indore 453552, India. E-mail: xray@iiti.ac.in; Tel: +91-7312438752

<sup>b</sup> Discipline of Biosciences and Bio-Medical Engineering, Indian Institute of Technology Indore, Simrol, Khandwa Road, Indore 453552, India

<sup>c</sup> Discipline of Metallurgy Engineering and Materials Science, Indian Institute of Technology Indore, Simrol, Khandwa Road, Indore 453552, India

† Electronic supplementary information (ESI) available. See DOI: 10.1039/d0ma00303d



great importance for the construction of highly efficient electrodes for sensing applications.

Herein, we have synthesized a novel pyramid shaped  $\text{CaTiO}_3$  perovskite structure using a hydrothermal method and employed it as an electrode material for the electrochemical sensing of urea. To the best of our knowledge, this is the first report on the use of  $\text{CaTiO}_3$  as electrode materials for urea sensing applications using electrochemical approaches.

## 2. Materials and methods

### 2.1. Chemicals and reagents

Calcium nitrate ( $\text{Ca}(\text{NO}_3)_2 \cdot 4\text{H}_2\text{O}$ ), titanium(IV) butoxide, phosphate buffered saline solutions, sodium hydroxide ( $\text{NaOH}$ ), polyvinylpyrrolidone, urea, hydrogen peroxide ( $\text{H}_2\text{O}_2$ ), ascorbic acid, uric acid, catechol, resorcinol, phenol, dopamine, glucose and other solvents were purchased from Merck, Sigma, SRL, Alfa Aesar and Fischer Scientific, India. All the purchased chemicals/reagents were used without any further purification.

### 2.2. Synthesis of $\text{CaTiO}_3$ pyramids

An aqueous solution (10 mL) of 4 M  $\text{Ca}(\text{NO}_3)_2 \cdot 4\text{H}_2\text{O}$  (9.446 gm) and 0.4 mL of titanium butoxide ( $\text{Ti(OBu)}_4$ ) were mixed in a round bottom flask slowly, stirred (rpm = ~900) for 10 min. 6 gm of sodium hydroxide dissolved in deionized water (15 mL) was added dropwise to the reaction mixture and stirred continuously for 30 min. Finally the reaction mixture was transferred to a 50 mL Teflon-lined stainless steel autoclave and heated for 24 h at 180 °C. The white precipitate was collected by centrifugation and washed with 1 M acetic acid and D.I. water several times to remove the unreacted residues.

### 2.3. Preparation of GC-1 and GC-2 electrodes

The active surface area of a glassy carbon (GC) electrode was cleaned with 0.5  $\mu\text{m}$  alumina slurry and washed with D.I. water.  $\text{CaTiO}_3$  pyramids were dispersed in D.I. water (1 mg  $\text{mL}^{-1}$ ) using an ultra-sonication bath for 1 h. The active surface area (3 mm = 0.07  $\text{cm}^2$ ) of the GC was modified with 10  $\mu\text{L}$  of  $\text{CaTiO}_3$  pyramids. 1 mg of urease was dissolved in 1 mL of PBS

( $\text{pH} = 7.0$ ) and 10  $\mu\text{L}$  of urease was drop cast on to the  $\text{CaTiO}_3$  pyramid modified GC electrode to obtain a thin film of urease. Finally 5  $\mu\text{L}$  of 1% polyvinylpyrrolidone (PVP) was also drop cast on to the modified GC ( $\text{GC/CaTiO}_3/\text{urease}$ ) as a binder. The electrode was kept to dry in air for 4 h. For a controlled experiment, we have modified the GC electrode with urease/PVP. All the modified electrodes were kept in a refrigerator before electrochemical measurements.

## 3. Results and discussion

### 3.1. Synthesis of $\text{CaTiO}_3$ pyramids

$\text{CaTiO}_3$  pyramids were synthesized by mixing calcium nitrate and titanium butoxide in basic medium ( $\text{NaOH}$ ) at 180 °C for 24 h by applying hydrothermal conditions to the reaction mixture (Scheme 1).

### 3.2. Physiochemical characterization

The powder X-ray diffraction (PXRD) investigation of the synthesized  $\text{CaTiO}_3$  was carried out using a RINT 2500V X-ray diffractometer (Rigaku, Japan;  $\text{Cu K}\alpha$  irradiation;  $\lambda = 1.5406 \text{ \AA}$ ). Fig. 1 displays the recorded PXRD pattern of the synthesized  $\text{CaTiO}_3$  in the  $2\theta$  range of 20–80°. The eight major diffraction peaks observed at 23.03°, 32.83°, 38.7°, 40.43°, 47.30°, 59.06°, 69.27° and 78.72° corresponded to the (110), (112), (103), (211), (220), (204), (224) and (116) planes, respectively. The PXRD results were consistent with previously reported literature (JCPDS no. 86-1393).<sup>17,28</sup> The highly intense diffraction peaks suggested the highly crystalline nature of the synthesized  $\text{CaTiO}_3$ . The average crystallite size of the synthesized  $\text{CaTiO}_3$  was calculated by employing the Debye–Scherrer formula as given in eqn (1) and the average crystallite size of the synthesized  $\text{CaTiO}_3$  was found to be 96.5 nm.

$$D = \frac{0.9\lambda}{\beta \cos \theta} \quad (1)$$

(Herein  $\beta$  = the broadening of the diffraction line while  $\lambda = 2.2897 \text{ \AA}$ )

Further, a Fourier-transform infrared (FTIR) spectroscopic investigation was conducted on a Bio-Rad FTS 300 MX to



Scheme 1 Schematic representation of the synthesis of  $\text{CaTiO}_3$  pyramids.



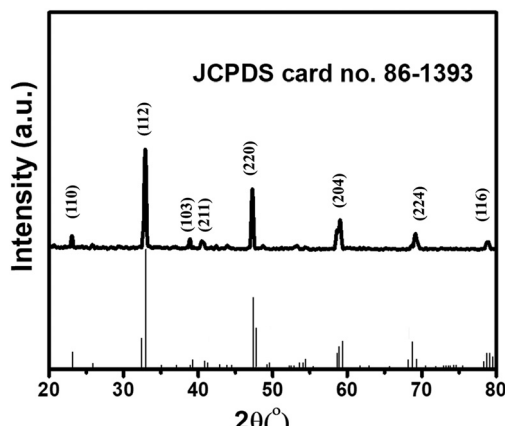


Fig. 1 PXRD pattern of  $\text{CaTiO}_3$  pyramids.

understand the presence of chemical bonds in the synthesized  $\text{CaTiO}_3$  (Fig. 2). Fig. 2 shows the recorded FTIR spectrum of the synthesized  $\text{CaTiO}_3$  in the wavelength range of  $4000\text{--}400\text{ cm}^{-1}$ . The bands appearing at  $3443$  and  $1639\text{ cm}^{-1}$  were due to the O-H stretching vibration and deformation of chemisorbed water molecules.<sup>18</sup>

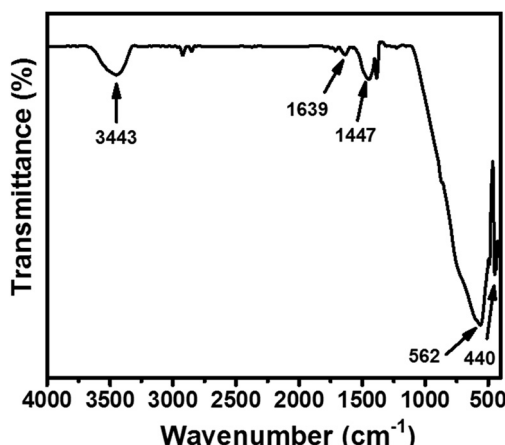


Fig. 2 FTIR of  $\text{CaTiO}_3$  pyramids.

The band at  $1447\text{ cm}^{-1}$  is assigned to the  $\text{CO}_3^{2-}$  bending vibration.<sup>29</sup> The band appearing at  $440\text{ cm}^{-1}$  may be assigned to the stretching vibration of Ti-O, whereas the band at  $562\text{ cm}^{-1}$  may be attributed to bridging stretching of Ti-O-Ti.<sup>18</sup> This also showed the presence of a  $\text{TiO}_6$  octahedral environment in the perovskite with  $\text{ABO}_3$  structure. The obtained FTIR spectrum was found to be in good agreement with previously reported data.<sup>18,29</sup>

The morphological features of nanomaterials can be affected by the solvent precursor, reaction times, temperature, pH and reactant concentration. It has also been reported that the crystallization mass transport and growth rate of the formation of  $\text{CaTiO}_3$  can be governed by the reactant concentration. Previously,  $\text{CaTiO}_3$  with butterfly-like dendrites was reported by using water,<sup>25</sup> whereas hollow cubic  $\text{CaTiO}_3$  was obtained with polyethylene glycol (PEG) as a solvent.<sup>26</sup> This showed that the solvent largely influences the particle surface morphology. In the present study,  $\text{CaTiO}_3$  pyramids were grown using water as a solvent. The particle surface morphology of the synthesized  $\text{CaTiO}_3$  was checked on an Oxford Instruments X-max, Aztec (Supra 55 Zeiss Field Emission Scanning Electron Microscope = FE-SEM). The recorded FE-SEM images of  $\text{CaTiO}_3$  have been displayed in Fig. 3 and Fig. S1 (ESI†). The FE-SEM results confirmed the pyramid like surface morphology of  $\text{CaTiO}_3$ . The  $\text{CaTiO}_3$  pyramids were grown in a uniform and smooth manner as suggested by the FE-SEM results. To the best of our knowledge, the hydrothermal growth of  $\text{CaTiO}_3$  with a pyramid like surface morphology has been achieved for the first time. The exact growth mechanism is not clear but we believe that NaOH may play a significant role in achieving  $\text{CaTiO}_3$  pyramids. Nucleation/accumulation was observed at the initial stages (2–4 h) as shown in Fig. S1A and B (ESI†). From 8–18 h, it started to grow in pyramid like structures (Fig. S1C–E, ESI†) and was completely transformed into pyramids of  $\text{CaTiO}_3$  after 24 h (Fig. S1F, ESI†).

The presence of the elements in  $\text{CaTiO}_3$  was determined on an energy dispersive X-ray (EDX) spectroscope (Oxford Instruments X-max, Aztec). The elemental spectrum and mapping images of Ca, Ti and O have been presented in Fig. 4A–D, respectively. The EDX investigation confirmed the presence of Ca, Ti and O elements in the  $\text{CaTiO}_3$  pyramids. Further, the surface area of the synthesized  $\text{CaTiO}_3$  was calculated by conducting an  $\text{N}_2$  adsorption–desorption

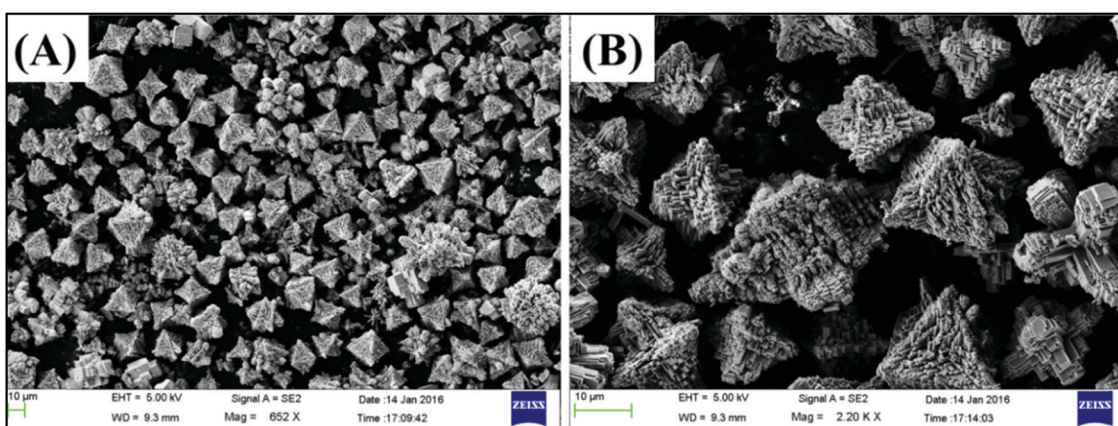


Fig. 3 FE-SEM images of  $\text{CaTiO}_3$  pyramids.



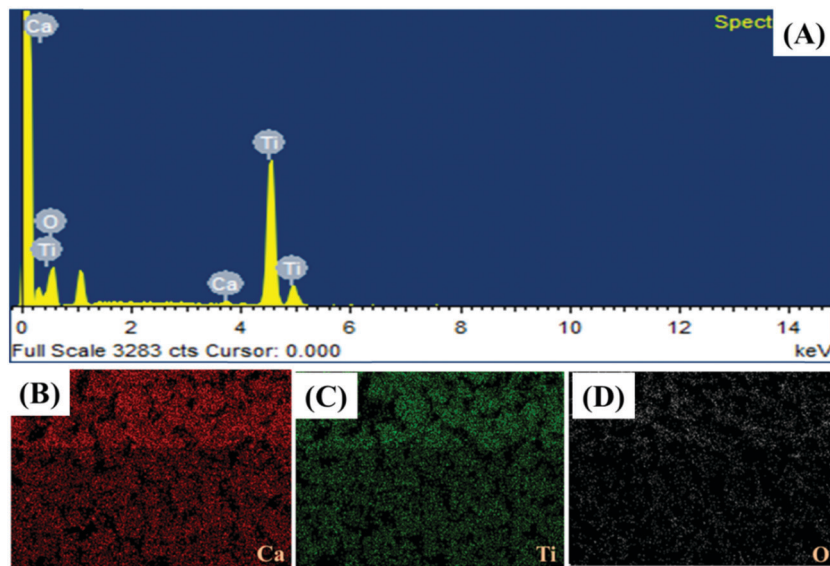


Fig. 4 EDX analysis of  $\text{CaTiO}_3$  pyramids.

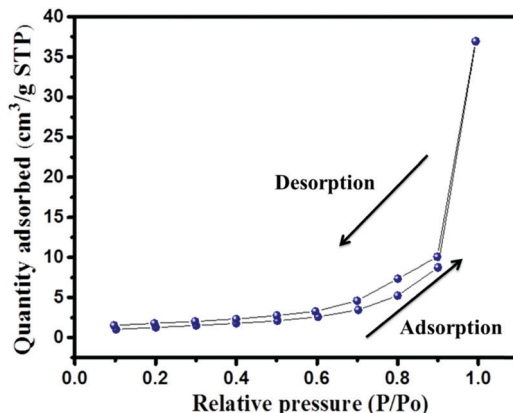


Fig. 5  $\text{N}_2$  adsorption–desorption curve of  $\text{CaTiO}_3$  pyramids.

investigation by using the Brunauer–Emmett–Teller (BET) approach (Autosorb iQ version 1.11; Quantachrome Instruments). The obtained adsorption–desorption curve of the synthesized  $\text{CaTiO}_3$  has been displayed in Fig. 5.

The specific surface area of the synthesized  $\text{CaTiO}_3$  was deduced to be  $67.5 \text{ m}^2 \text{ g}^{-1}$  (Fig. 5). Hence, it can be proposed that the  $\text{CaTiO}_3$  perovskite with interesting surface morphology and good surface area may be useful in electrochemical applications. Therefore, we have employed the prepared  $\text{CaTiO}_3$  pyramids as an electrode modifier for the determination of urea.

### 3.3. Electrochemical measurements

The electrochemical measurements were carried out on a computer controlled Metrohm Autolab PGSTAT 302N with a three electrode system. The GC electrode was used as the working electrode substrate while platinum wire and  $\text{Ag}/\text{AgCl}$  were used as the counter and reference electrode, respectively. The non-modified GC electrode is denoted as bare GC whereas the GC electrode modified with  $\text{CaTiO}_3$  pyramids/urease/PVP has been

denoted as GC-2. The GC electrode modified with urease/PVP is denoted as GC-1.

The charge transfer characteristics of the bare GC and GC-2 were investigated using electrochemical impedance spectroscopic (EIS) study. The recorded Nyquist plots of the bare GC and GC-2 were recorded in the presence of  $2 \text{ mM} [\text{Fe}(\text{CN})_6]^{3-/-4-}$  in  $0.1 \text{ M PBS}$  ( $\text{pH} = 7.0$ ) with an applied frequency range of  $0.01 \text{ Hz}$ – $100 \text{ kHz}$ . Fig. 6 shows the plotted Nyquist plot between the imaginary impedance ( $-Z''$ ) and real impedance ( $Z'$ ). From Fig. 6, it can be seen that the bare GC has high charge resistance whereas GC-2 possesses lower charge resistance. It is well understood that high charge resistance limits the electron transport or electron transfer process. This suggested that GC-2 has good electron transport ability compared to the bare GC due to its low charge resistance.

The cyclic voltammetry (CV) and current–voltage ( $I$ – $V$ ) approaches were used to probe the electrochemical behavior of GC-2. The CV curves of the bare GC and GC-2 were recorded in the presence of

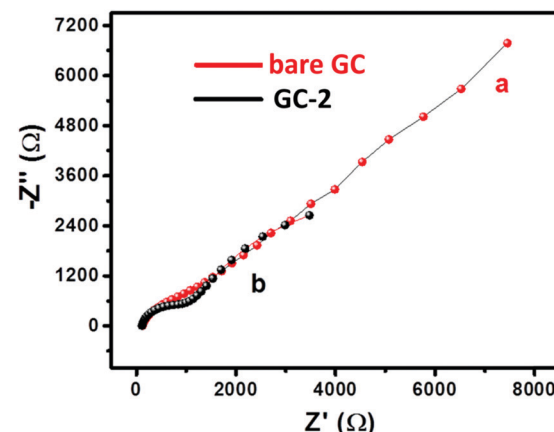


Fig. 6 Nyquist plot of (a) the bare GC and (b) GC-2 in  $2 \text{ mM} [\text{Fe}(\text{CN})_6]^{3-/-4-}$  solution in  $0.1 \text{ M PBS}$  ( $\text{pH} = 7.0$ ).



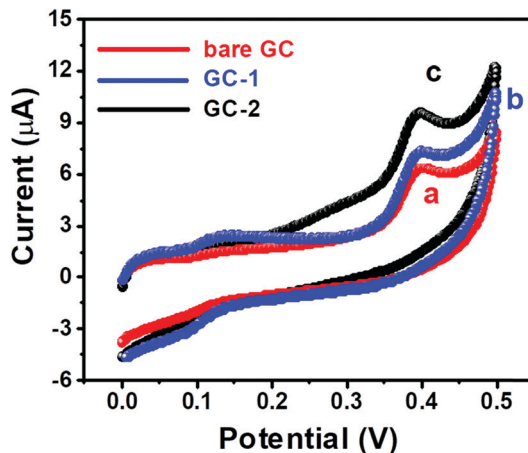


Fig. 7 CV curves of (a) the bare GC, (b) GC-1 and (c) GC-2 in the presence of 250  $\mu\text{M}$  urea in 0.1 M PBS ( $\text{pH} = 7.0$ ) at an applied scan rate of  $0.1 \text{ V s}^{-1}$ .

250  $\mu\text{M}$  urea in 0.1 M PBS ( $\text{pH} = 7.0$ ) with an applied scan rate of  $0.1 \text{ V s}^{-1}$ . The bare GC showed a current response of 6.3  $\mu\text{A}$  whereas GC-2 showed 9.8  $\mu\text{A}$  towards the oxidation of 250  $\mu\text{M}$  urea (Fig. 7). This high current response of GC-2 suggested the successful surface modification of the GC-2 electrode and better electro-catalytic activity towards the oxidation of urea compared to the bare GC. We have also recorded the CV curve of GC-1 to check the reason for this enhanced current response of 9.8  $\mu\text{A}$ . GC-1 exhibited a relatively high current response (7.3  $\mu\text{A}$ ) compared to the bare GC, which is due to the presence of catalytic properties in the urease. However, this current response was lower compared to GC-2. This showed that the presence of  $\text{CaTiO}_3$  pyramids with urease significantly enhanced the current response.

Further,  $I$ - $V$  curves of the bare GC and GC-2 were also recorded in the presence of 250  $\mu\text{M}$  urea in 0.1 M PBS ( $\text{pH} = 7.0$ ) with an applied scan rate of  $0.1 \text{ V s}^{-1}$  (Fig. 8).

The bare GC showed a current response of 8.9  $\mu\text{A}$ , while GC-2 exhibited a higher current response of 19.51  $\mu\text{A}$ . The obtained results showed a similar trend that GC-2 has high electro-catalytic ability for the oxidation of urea. Moreover, it was also observed that GC-2 showed a current response of 8.9  $\mu\text{A}$

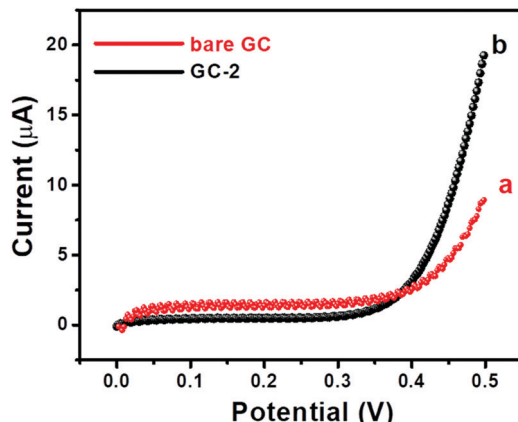


Fig. 8  $I$ - $V$  curves of (a) the bare GC and (b) GC-2 in the presence of 250  $\mu\text{M}$  urea in 0.1 M PBS ( $\text{pH} = 7.0$ ).

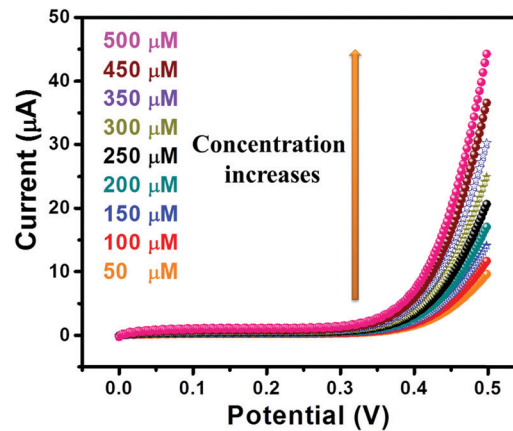


Fig. 9  $I$ - $V$  curves of GC-2 in different concentrations (50–500  $\mu\text{M}$ ) of urea in 0.1 M PBS ( $\text{pH} = 7.0$ ).

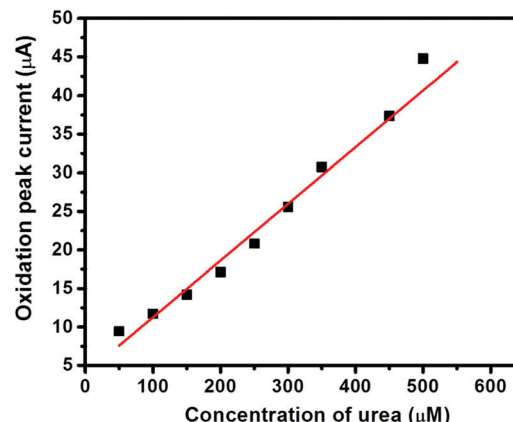


Fig. 10 Calibration plot of the current peaks against the concentrations of urea.

using CV whereas 19.51  $\mu\text{A}$  was obtained using the  $I$ - $V$  technique. Thus, it can be said that the  $I$ - $V$  approach is more sensitive in this case. Hence, we have conducted  $I$ - $V$  measurements for further electrochemical probes and investigations. The effects of different concentrations of urea on the electrochemical performance of GC-2 were determined by using the  $I$ - $V$  approach.

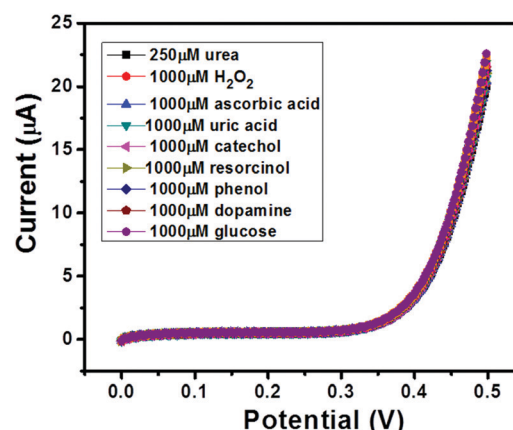


Fig. 11  $I$ - $V$  curves of GC-2 in the presence of urea (250  $\mu\text{M}$ ) in 0.1 M PBS ( $\text{pH} = 7.0$ ) with different interfering species (1000  $\mu\text{M}$ ).



The *I*-*V* curves of GC-2 in the presence of different concentrations (50–500  $\mu$ M) of urea in 0.1 M PBS were recorded (Fig. 9). The obtained results showed that the current response was enhanced with increasing the concentration of urea. The linear calibration plot of the current peaks against the concentrations of urea has been presented in Fig. 10. The increase of the current response was found to be linear with respect to the concentration of urea (Fig. 10).

### 3.4. Selectivity and repeatability studies

The selectivity of a sensor has always been a major concern due to the availability of various electro-active species (such as glucose, uric acid *etc.*) which may affect the electrochemical performance of the sensor in terms of accuracy. Thus, an ideal sensor should be

highly selective. We have performed selectivity studies in the presence of ascorbic acid, hydrogen peroxide, uric acid, catechol, resorcinol, phenol, dopamine and glucose. The *I*-*V* curves of GC-2 were recorded in the presence of 250  $\mu$ M in 0.1 M PBS (pH = 7.0) with interfering species (conc.; 1000  $\mu$ M) and the obtained results are shown in Fig. 11. There was no significant change in the current response observed even when the concentrations of the electro-active species were 4 times higher than that of urea. Thus, it revealed the good selectivity of GC-2 towards urea sensing.

Furthermore, the repeatability of the sensor is also an important tool; therefore, we have recorded 5 consecutive *I*-*V* curves of GC-2 in the presence of 250  $\mu$ M urea in 0.1 M PBS (pH = 7.0). The recorded *I*-*V* curves have been presented in Fig. 12. There was an insignificant change in the current response observed, which indicated its remarkably good repeatability.

The detection limit of the GC-2 based urea sensor was calculated using the following eqn (2)<sup>21</sup>

$$\text{Detection limit (LOD)} = 3.3 \times \sigma/S \quad (2)$$

where  $\sigma$  = standard error while  $S$  = slope of the calibration curve. The detection limit of the GC-2 based urea sensor was found to be  $1.6 \pm 0.2 \mu\text{M}$  with a linear range of 50–450  $\mu\text{M}$ . The sensitivity was found to be  $0.9 \mu\text{A } \mu\text{M}^{-1} \text{ cm}^{-2}$  using the formula sensitivity = slope/area of the electrode. The electrochemical oxidation of urea can be represented as shown in Scheme 2. This probable mechanism has been proposed according to previously reported literature.<sup>30–33</sup> The electrochemical oxidation of urea probably produced  $\text{NH}_3$  and  $\text{CO}_2$  as shown in Scheme 2.

### 3.5. Comparison

Since the performance of the electrochemical sensor depends on various factors including the nature and quality of the electrode modifiers, hence we have compared the performance of GC-2 with previously reported literature. Mondal *et al.*<sup>30</sup> employed polypyrrole/Pt as an electrode material for the sensing of urea with a detection limit of 40  $\mu\text{M}$ . Nguyen *et al.*<sup>31</sup> synthesized 3D-graphene/ $\text{NiCo}_2\text{O}_4$  and constructed a urea sensor showing a limit of detection of 5  $\mu\text{M}$ . Nguyen *et al.*<sup>32</sup> also constructed a urea sensor based on a NiO/cellulose/CNT electrode modifier which showed a detection limit of 7  $\mu\text{M}$ . Tak *et al.*<sup>33</sup> used a ZnO-MWCNT composite whereas Srivastava *et al.*<sup>34</sup> employed a  $\text{TiO}_2$ - $\text{ZrO}_2$  composite for the sensing of urea, but the obtained detection limit was poor. Different electrode modifiers have been developed for urea sensing.<sup>16,35</sup> In particular,

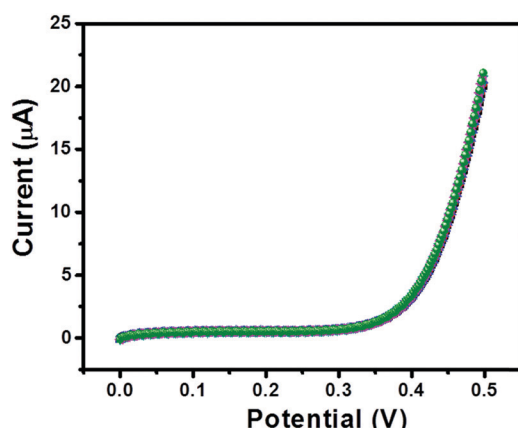
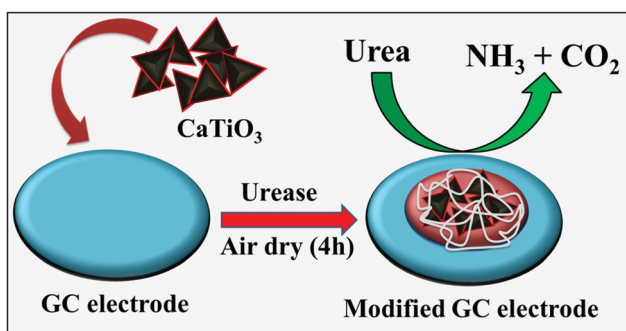


Fig. 12 Five consecutive *I*-*V* curves of GC-2 in the presence of urea (250  $\mu\text{M}$ ) in 0.1 M PBS (pH = 7.0).



Scheme 2 Schematic illustration of urea sensing.

Table 1 Comparison table of the GC-2 based urea sensor with previously reported sensors

S. no.	Electrode modifier	Detection limit ( $\mu\text{M}$ )	Sensitivity ( $\mu\text{A } \mu\text{M}^{-1} \text{ cm}^{-2}$ )	Electrode diameter ( $\text{cm}^2$ )	Ref.
1	Polypyrrole/Pt	40	1.11 $\mu\text{A } \mu\text{M}^{-1} \text{ cm}^{-2}$	0.03	30
2	3D-graphene/ $\text{NiCo}_2\text{O}_4$	5	166	0.25	31
3	NiO/cellulose/CNT	7	371	0.25	32
4	ZnO-MWCNT composite	230	43.02	0.25	33
5	$\text{TiO}_2$ - $\text{ZrO}_2$ composite	440	2.74	0.25	34
6	(Fc-PAMAM) dendrimers/MWCNTs	50	1.085	—	35
7	ZnO NRs	10	41.64	—	16
8	Vitamin C based NiO	10	—	—	36
9	Ni-MOF/Nafion/GCE	2.23	118.77	—	15
10	$\text{NiCo}_2\text{O}_4$ nanoneedles	1	—	0.03	37
11	GC-2	1.6	0.9 $\mu\text{A } \mu\text{M}^{-1} \text{ cm}^{-2}$	0.07	This work



Arain *et al.*<sup>36</sup> used vitamin C based NiO as a urea sensor which exhibited a detection limit of 10  $\mu\text{M}$ . Bao *et al.*<sup>15</sup> used a novel composite of a metal-organic-framework (Ni-MOF/Nafion/GCE) for urea sensing with a good detection limit of 2.23  $\mu\text{M}$ . Amin *et al.*<sup>37</sup> investigated the electrochemical behavior of  $\text{NiCo}_2\text{O}_4$  nanoneedles towards the sensing of urea and obtained a detection limit of 1  $\mu\text{M}$ . The obtained detection limit in the present work is comparable with the previous reports as shown in Table 1.<sup>15,16,30-37</sup>

## 4. Conclusion

Pyramid shaped  $\text{CaTiO}_3$  was synthesized using a hydrothermal method. A glassy carbon electrode was modified by drop casting of  $\text{CaTiO}_3$  and urease to prepare the working electrode (GC-2). This prepared GC-2 electrode was employed for the determination of urea by employing voltammetric approaches. The developed GC-2 electrode exhibited a good detection limit and high selectivity towards urea sensing. Moreover, we believe that GC-2 can also be used in other applications such as fuel cells, supercapacitors or water splitting.

## Conflicts of interest

There are no conflicts to declare.

## Acknowledgements

K. A. and P. K. thank the University Grant Commission and DST-Inspire, New Delhi, India, for providing fellowships, respectively. The authors acknowledge Sophisticated Instrumentation Centre (SIC) and Department of Chemistry, IIT Indore, for providing the characterization facility. S. M. M. thanks CSIR (01(2935)/18/EMR-II) and SERB-DST (EMR/2016/001113), New Delhi, India, and IIT Indore for financial support.

## References

- D. Dutta, S. Chandra, A. K. Swain and D. Bahadur, *Anal. Chem.*, 2014, **86**, 5914–5921.
- M. Tyagi, M. Tomar and V. Gupta, *Biosens. Bioelectron.*, 2013, **41**, 110–115.
- J. Yoon, D. Lee, E. Lee, Y. S. Yoon and D.-J. Kim, *Electroanal.*, 2019, **31**, 17–21.
- Y.-L. Liu, R. Liu, Y. Qin, Y. Qin, Y. Qin, Q.-F. Qiu, Z. Chen, S.-B. Cheng and W.-H. Huang, *Anal. Chem.*, 2018, **90**, 13081–13087.
- K. Ahmad, P. Kumar and S. M. Mobin, *Nanoscale Adv.*, 2020, **2**, 502–511.
- W. Raza and K. Ahmad, *Mater. Lett.*, 2018, **212**, 231–234.
- K. Ahmad and S. M. Mobin, *Nanoscale Adv.*, 2019, **1**, 719–727.
- K. Ahmad, P. Kumar and S. M. Mobin, *J. Electrochem. Soc.*, 2019, **166**, B1577–B1584.
- K. Ahmad and S. M. Mobin, *J. Environ. Chem. Eng.*, 2019, **7**, 103347.
- K. Ahmad, A. Mohammad and S. M. Mobin, *Electrochim. Acta*, 2017, **252**, 549–557.
- Z. Parsaee, *Ultrason. Sonochem.*, 2018, **44**, 120–128.
- M. Mikani, S. Talaei, R. Rahamanian, P. Ahmadi and A. Mahmoudi, *J. Electroanal. Chem.*, 2019, **840**, 285–294.
- R. Sha, K. Komori and S. Badhulika, *Electrochim. Acta*, 2017, **233**, 44–51.
- T. S. S. K. Naik, S. Saravanan, K. N. S. Saravana, U. Pratiush and P. C. Ramamurthy, *Mater. Chem. Phys.*, 2020, **245**, 122798.
- C. Bao, Q. Niu, Z.-A. Chen, X. Cao, H. Wang and W. Lu, *RSC Adv.*, 2019, **9**, 29474–29481.
- R. Ahmad, N. Tripathy and Y.-B. Hahn, *Sens. Actuators, B*, 2014, **194**, 290–295.
- S. Som, A. K. Kunti, V. Kumar, V. Kumar, S. Dutta, M. Chowdhury, S. K. Sharma, J. J. Terblans and C. Swart, *J. Appl. Phys.*, 2014, **115**, 193101.
- Y. Wang, C.-G. Niu, L. Wang, Y. Wang, X.-G. Zhang and G.-M. Zeng, *RSC Adv.*, 2016, **6**, 47873–47882.
- J. Staniforth, S. E. Evans, O. J. Good, R. J. Darton and R. M. Ormerod, *Dalton Trans.*, 2014, **43**, 15022–15027.
- X. He, C. Hu, Y. Xi, B. Wan and C. Xia, *Sens. Actuators, B*, 2009, **137**, 62–66.
- K. Ahmad, A. Mohammad, P. Mathur and S. M. Mobin, *Electrochim. Acta*, 2016, **215**, 435–446.
- K. Ahmad, P. Kumar and S. M. Mobin, *Nanoscale Adv.*, 2020, **2**, 502–511.
- B. Muthukutty, R. Karthik, S.-M. Chen and M. Abinaya, *New J. Chem.*, 2019, **43**, 12264–12274.
- T. Kimijima, K. Kanie, M. Nakaya and A. Muramatsu, *CrystEngComm*, 2014, **16**, 5591–5597.
- W. Dong, G. Zhao, B. Song, G. Xu, J. Zhou and G. Han, *CrystEngComm*, 2012, **14**, 6990–6997.
- X. Yang, J. Fu, C. Jin, J. Chen, C. Liang, M. Wu and W. Zhou, *J. Am. Chem. Soc.*, 2010, **132**, 14279–14287.
- D. Wang, Z. Guo, Y. Chen, J. Hao and W. Liu, *Inorg. Chem.*, 2007, **46**, 7707–7709.
- G. Dong, X. Xiao, L. Zhang, Z. Ma, X. Bao, M. Peng, Q. Zhang and J. Qiu, *J. Mater. Chem.*, 2011, **21**, 2194–2203.
- H. K. Yang, J. W. Chung, G. S. R. Raju, B. K. Moon, B. C. Choi, J. H. Jeong and J. H. Kim, *Appl. Surf. Sci.*, 2009, **255**, 5062–5066.
- S. Mondal and M. V. Sangaranarayanan, *Sens. Actuators, B*, 2013, **177**, 478–486.
- N. S. Nguyen, G. Das and H. H. Yoon, *Biosens. Bioelectron.*, 2016, **77**, 372–377.
- N. S. Nguyen and H. H. Yoon, *Sens. Actuators, B*, 2016, **236**, 304–310.
- M. Tak, V. Gupta and M. Tomar, *J. Mater. Chem. B*, 2013, **1**, 6392–6401.
- S. Srivastava, A. Ali, P. R. Solanki, P. M. Chavhan, M. K. Pandey, A. Mulchandani, A. Srivastava and B. D. Malhotra, *RSC Adv.*, 2013, **3**, 228–235.
- D. Esma, D. Muamer, N. N. Jackson and S. Mehmet, *Sens. Actuators, B*, 2017, **246**, 920–926.
- M. Arain, A. Nafady, Sirajuddin, Z. H. Ibupoto, S. T. H. Sherazi, T. Shaikh, H. Khan, A. Alsalme, A. Niaz and M. Willander, *RSC Adv.*, 2016, **6**, 39001–39006.
- S. Amin, A. Tahira, A. Solangi, V. Beni, J. R. Morante, X. Liu, M. Falhman, R. Mazzaro, Z. H. Ibupoto and A. Vomiero, *RSC Adv.*, 2019, **9**, 14443–14451.

